Hot-electron photodynamics in silver-containing BEA-type nanozeolite studied by femtosecond transient absorption spectroscopy

Farah Kawtharani, Svetlana Mintova, Richard Retoux, Mehran Mostafavi, Guy Buntinx, Vincent de Waele

Hot-electron photodynamics in silver-containing BEA-type nanozeolite studied by femtosecond transient absorption spectroscopy

Farah Kawtharani,[a,b] Svetlana Mintova,[b] Richard Retoux,[c] Mehran Mostafavi,[d] Guy Buntinx,[a] Vincent De Waele,[a]*

Dedication Dedicated to the memory of our esteemed colleague Dr Olivier Poizat

[a] Dr F. Kawtharani, Dr G. Buntinx, Dr V. De Waele
Univ. Lille, CNRS
UMR 8516, LASIRE–Laboratoire de Spectroscopie pour les Interactions, la Réactivité et l'Environnement
F-59000 Lille, France,
E-mail: Vincent.de-waele@univ-lille.fr
[b] Dr S. Mintova, Dr F. Kawtharani
Normandie Université,
Laboratoire Catalyse et Spectrochimie (LCS),
ENSICAEN, UNICAEN, CNRS,
6 boulevard Maréchal Juin, Caen 14050, France
[c] Dr R. Retoux
Laboratoire CRISMAT UMR 6508 ENSICAEN,
6 Bd du Maréchal Juin 14050 Caen Cedex 4
[d] Pr M. Mostafavi
Institut de Chimie Physique,
Université Paris-Saclay, CNRS,
Orsay, 91405, France

Supporting information for this article is given via a link at the end of the document: BET, XRD, HRTEM and additional UV-vis characterizations, Additional sets of transient data and fits of the pump-probe decays.

Abstract: Silver cations were introduced in nanosized BEA-type zeolite containing organic template by ion-exchange followed by chemical reduction towards preparation of photoactive materials (Ag^0-BEA). The stabilization of highly dispersed Ag^0 nanoparticles with a size of 1-2 nm in the BEA zeolite was revealed. The transient optical response of the Ag-BEA samples upon photoexcitation at 400 nm was studied by femtosecond absorption. The photodynamic of the hot electrons was found to depend on the sample preparation. The lifetime of the hot electrons in the Ag-BEA samples containing small Ag nanoparticles (1-2 nm) is significantly shortened in comparison to bear Ag nanoparticles with a size of 10 nm. While for the larger Ag nanoparticles, the energy absorbed in the conduction band is decaying by electron-phonon coupling into the metal lattice, the high surface-to-volume ratio of the small Ag nanoparticles favors the dissipation of the energy of the hot electrons from the metal nanoparticles (Ag^0) towards the zeolitic micro-environment. This finding is encouraging for further applications of Ag-containing zeolites in photocatalysis and plasmonic chemistry.

Introduction

Zeolites are microporous crystalline solids constituted by a regular 3-dimensional arrangement of TO_4 groups (T = Si, Al) that form cages and channels with a size lower than 2 nm. The zeolite materials offer unique possibility to tailor the properties of photoactive guest chemical species[1–4], organo-metallic complexes[5,6], metal clusters and nanoparticles[7,8] by confining them inside the pores and aligning along their 3D architecture[9,10]. Metal-containing zeolites are notably investigated for photocatalysis[11–13] and one attractive route of development consists coupling of zeolites with plasmonic nanostructure to enhance their photocatalytic activity[14–16]. Plasmonic chemistry[17–20] is an emerging area of the photocatalysis that aims to exploit the photoexcitation of the electrons of metal nanoparticle to trigger chemical reactions at the surface of the metal nanoparticles. These processes occur in femtosecond-picosecond time-scale and they have been investigated by transient absorption spectroscopy[21–25]. The dynamics of the hot-electrons generated upon the absorption of photons has been characterized for metal nanoparticle of different sizes [21,24,26,27] and shapes, in weak and high perturbation regime, and different surrounding and surface interactions[28–30].

In view of these emerging plasmonic applications, we are interested in nanosized zeolites[31,32] with a size of 5-100 nm, that can be stabilized in transparent colloidal suspensions or assembled in thin films for light-driven applications. Nanozeolites were successfully functionalized by the incorporation of metallic[33,34] and semiconductor[35] nanoparticles (CdS, ZnS, CdSe) with different shapes and size using radiolysis[33,36,37], chemical[34,38] and photochemical[37,39] approaches. For most of the systems investigated, the synthesis conditions can be optimized to favor the stabilization of relatively small (1-3 nm) metal and semiconductor nanoparticles. Such very small supported nanoparticles are interesting for plasmonic applications because, in principle, the smaller the particles, the higher the density of energy acquired by the absorption of light. We verified this assumption in our previous study[40], where the hot electron dynamics of 1 nm-sized silver nanoparticles (Ag-NPs) stabilized in LTL type nanozeolite assembled in transparent thin films was studied. This study was performed on template-free LTL nanozeolite dehydrated under high vacuum. We demonstrated that highly excited electrons can be photogenerated in the zeolite film under low light illumination. In the case of small metallic nanoparticles supported in zeolites, the interactions at the surface of the metals with the zeolite or the molecules confined inside their porous volume, can impact the hot electron relaxations.

In the present work, the synthesis and the characterization of silver nanoparticles (Ag NPs) in two zeolite samples with a Si:Al ratio of 13 and 7.5 stabilized in aqueous colloidal suspensions is presented. The ultrafast optical response of these Ag-BEA samples to characterize the impact of the zeolite on the hot electron lifetime was elucidated.

Results

Characterization of the non-reduced Ag-containing zeolite suspensions

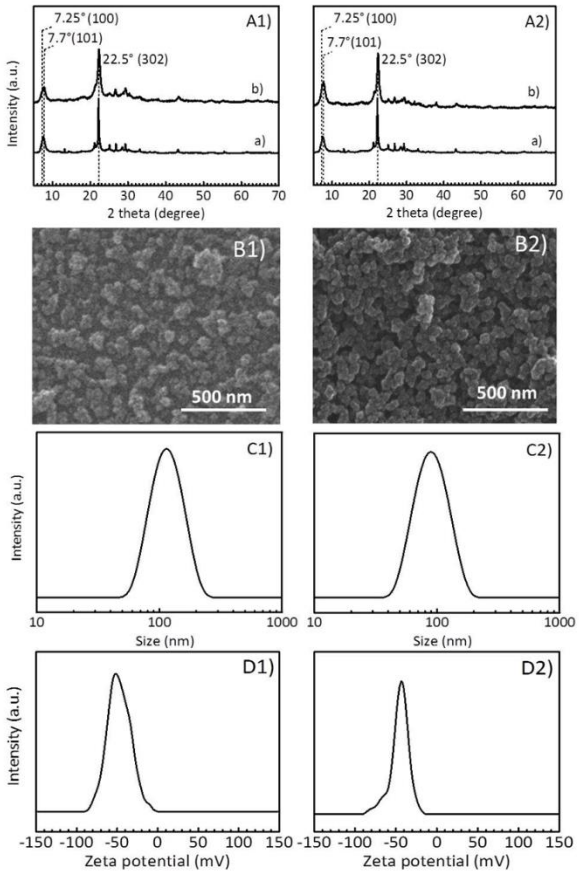

Figure 1. A1) X-ray diffraction patterns recorded of (a) parent BEA-1 nanosized zeolite and (b) ion exchanged Ag^+-BEA-1; B1) SEM picture, (C1) DLS curve, (D1) zeta potential curve recorded for sample Ag^+-BEA-1. A2) X-ray diffraction pattern recorded of (a) parent BEA-2 nanosized zeolite and (b) ion exchanged Ag^+-BEA-2, B2) SEM picture, (C2) DLS curve, (D2) zeta potential curve recorded for sample Ag^+-BEA-2.

The crystallinity of zeolite samples **BEA-1 and BEA-2** synthesized with two different Si/Al ratios was studied by X-ray diffraction (XRD). The XRD patterns of the samples are depicted in **Figure 1**. Both samples exhibit the Bragg reflections corresponding to the BEA-type framework structure, consisting of a broad peak composed of two peaks at 7.25°and 7.7° 2θ with Miller indices (hkl) of (100) and (101), respectively and a peak at 22.5° with *hkl* (302).[41] The broad peak at 7.7° 2θ indicates the presence of polymorphs A and B with an estimated ratio of 45:55.[42] No signatures of framework destruction or amorphization are detected after ion-exchange of the samples with silver (Figure 1). The SEM pictures show that the nanocrystals with a size of 10 nm are aggregated resulting in particles with an average size of 60-120 nm. The DLS curves reveal a monomodal particle size distribution with a mean hydrodynamic diameter of the aggregates of 114 nm (**Ag^+-BEA-1**) and 90 nm (**Ag^+-BEA-2**). The zeta potential values (ς) of -50mV and -45 mV for samples **Ag^+-BEA-1** and **Ag^+-BEA-2**, respectively confirmed the high stability of negatively surface charged nanoparticles.

Table 1: Chemical composition of ion exchanged Ag^+-BEA-1 and Ag^+-BEA-2 nanosized zeolite samples

	Si /Al	Al /u.c	TEA^+ /u.c.	H_2O /u.c.	Ag^+ wt%[a]	Ag^+ /u.c.	$[Ag^+]$[b]
Ag^+-BEA-1	7.5	7.5	3.8	2.1	3.4	1.2	2.5
Ag^+-BEA-2	13.1	4.5	4	10	1.4	0.5	0.78

[a] weight percentage per gram of zeolite. [b] mmol/L in suspension with a solid (zeolite) concentration of 0.8 wt%

The chemical composition of samples **Ag⁺-BEA-1** and **Ag⁺-BEA-2** determined by ICP is summarized in **Table 1**, while the amount of water and organic templates as determined by TG are presented in **Table 1** and **Figure 2**. The weight losses of the samples are described by considering 4 temperature ranges similarly presented for pure BEA[43–45]. For **Ag⁺-BEA-1**, in region 1 (25-150 °C) a peak assigned to desorption of zeolitic water is present. The decomposition of the organic template (TEA^+) from zeolite Beta is represented by the peak in the temperature interval (150-350 °C), Region 2. In region 3 (350-500 °C), a peak situated at 353°C and a less intense peak at 430°C, are present. These peaks are assigned to the degradation of the template located in the channels compensating the negative charges of the framework The peak observed in region 4 (500-750 °C) located at 550 °C is assigned to the burning of the residues formed in region 3 and tcomplete removal of the organics. For sample **Ag⁺-BEA-2**, similar results were obtained, however the small variation of the TG profile is an indication for the different amount of TEA^+ species, and consequently of the distribution and the chemical environment of Ag^+ cations inside the zeolite crystals. Samples **Ag⁺-BEA-1** and **Ag⁺-BEA-2** are different in the Ag^+ content due to the different Si/Al ratios of the BEA zeolites and they contain different amount of template and water (**Figure 2**).

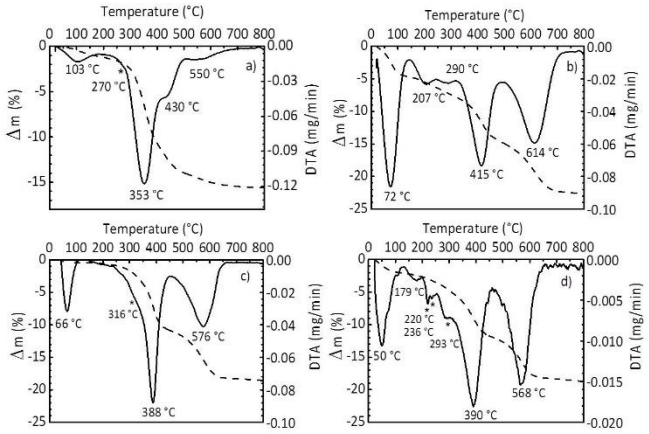

Figure 2. TG/DTG curves of a) Ag^+-BEA-1, b) Ag^+-BEA-2, c) Ag^0-BEA-1 and d) Ag^0-BEA-2 samples

Chemical reduction of Ag-containing zeolite suspensions by triethylamine

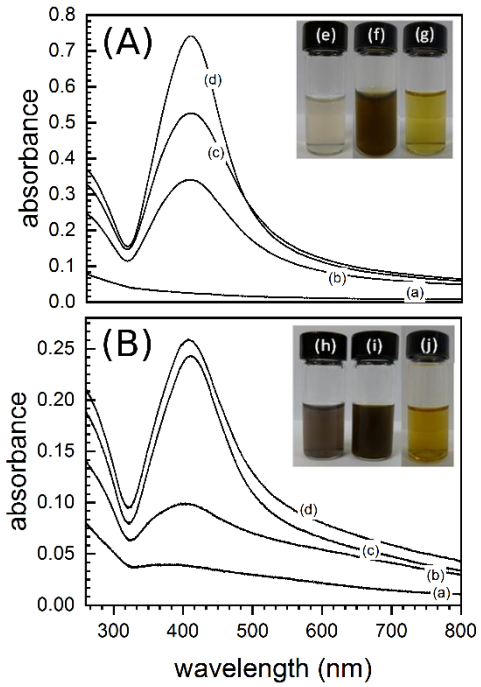

Figure 3. UV-vis spectra recorded for samples Ag^0-BEA-1 (A) and Ag^0-BEA-2 (B) during the chemical reduction process using triethylamine (Et_3N): (a) prior chemical reduction of Ag^+-BEA sample, (b) immediately after chemical reduction (c) after 1 hour and (d) after 24 hours. The molar concentration of silver in the suspensions Ag^0-BEA-1 and Ag^0-BEA-2 are 7.1×10^{-5} mol.l^{-1} and 2.25×10^{-5} mol.l^{-1}, respectively; inset pictures (g) and (j) correspondingly). Inset pictures (e) and (f) show samples Ag^+-BEA-1 (0.8wt%) and Ag^0-BEA-1 (0.8wt%), correspondingly. Insets (h) and (i) show pictures of samples Ag^+-BEA-2 (0.8wt%) and Ag^0-BEA-2 (0.8wt%), correspondingly.

The silver cations **(Ag^+)** were reduced to metal nanoparticles (Ag^0) in suspensions **Ag⁺-BEA-1** and **Ag⁺-BEA-2** subjected to reduction procedures A and B (see experimental section). The reduction process in the presence of triethylamine (Et_3N) has been directly followed

by UV-vis absorption owing to the transparency of the colloidal zeolite suspensions and to the strong plasmon absorption band of silver nanoparticles in the visible spectral range. For both samples, an excess amount of Et_3N (procedure A) was used for both **Ag^+-BEA-1** and **Ag^+-BEA-2** samples; well-defined absorption spectra containing a strong band at 410 nm and a second low intensity absorption band bellow 350 nm are presented in **Figure 3**. As a visual indication, the color of the suspensions turns from white-pale grey to yellow. In both samples, the initial pale-grey color is associated with a broad and weak absorption/diffusion spectrum corresponding to the ion-exchanged samples which is more intense for **Ag^+-BEA-2.**

The reduction kinetics for samples **Ag^+-BEA-1** and **Ag^+-BEA-2** differs noticeably (**Figure 3**). In sample **Ag^0-BEA-1,** the plasmon band at 410 nm and the width of the band is slightly diminishing during the formation of the Ag^0 nanoparticle, as it is usually reported for nm-sized spherical Ag-NPs[46]. A similar spectral evolution for **Ag^0 BEA-2** is observed but with an asymmetry of the plasmon band featuring more intense tail in the red-part of the spectra. That second contribution cannot be assigned directly. This feature is expected for large (>20 nm) or non-spherical nanoparticles, or in case of inter-particles interactions resulting from the confinement of Ag NPs in the Beta zeolite matrix. Alternatively, this asymmetry might reflect specific electronic interactions between the metal nanoparticles and their micro-environment.
The stability of the zeolite framework was further confirmed by recording the N2 sorption isotherms, XRD patterns and TEM images. Nitrogen adsorption-desorption measurements confirmed that the microporosity of the BEA zeolite is preserved after the chemical reduction (see SI, Figure 1). The XRD patterns show that the crystallinity of the **Ag^0-BEA-1** and **Ag^0 BEA-2** samples is preserved (see SI-Figure 2). In addition, the TEM images of the reduced samples reveal the crystalline fringes of BEA zeolite (SI-Figure 3). In summary, the BEA zeolite samples under the mild reduction conditions stayed intact.

To confirm the presence of Ag NPs in the BEA zeolite matrix, STEM and HAADF images were recorded (**Ag^0 BEA-2).** The contrast of the HAADF image is determined by the atomic number (Z-contrast) of the elements in the sample. The Ag NPs are evidenced as bright dots (due to their high Z) randomly distributed in the zeolite sample (low Z-contrast, due to lighter elements) that appears as more or less grey/background. The silver nanoparticles embedded within the zeolite matrix are highly dispersed (**Figure 4**). The chemical composition of two selected areas of sample **Ag^0-BEA-2** are presented in **Figure 4**. Two measurements are performed; on bright zone of the sample labelled as zone A1, and the other darker zone labelled as zone A2 (**Figure 4)**. The EDS spectrum of the bright zone (zone A1) confirms the Ag nanoparticles; the Si peak which is the main constituent of the zeolite structure (except C and O), and another peak of Ag are present. On the contrary, the grey/dark zone pointed by zone A2 contains only a peak of Si, and no Ag peak was measured revealing the pure zeolite. Additional HRTEM images of **Ag^0-BEA-1** and **Ag^0-BEA-2** (see SI-Figure 3) confirmed the formation of nm-sized Ag NPs (1-2 nm) in the BEA zeolite matrix.
The as-prepared suspensions are transparent over the visible spectral range and stable for months (SI-Figure 5).

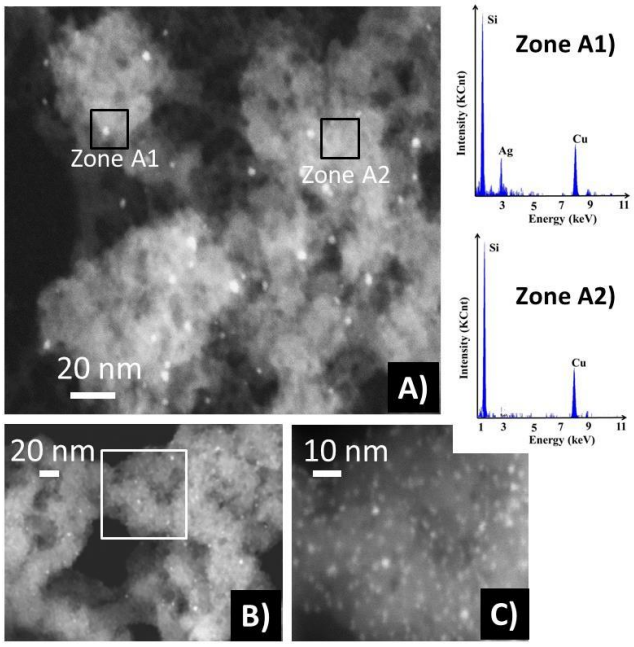

Figure 4. A) HAADF images coupled with the point EDS technique of colloidal Ag^0-BEA-2, performed at two selected zones A1 and A2. The contrast of the HAADF image is identified by the atomic number Z-contrast: Ag NPs are visualized as bright dots due to the high atomic number, and the zeolite matrix as a dark background due to its low Z-contrast. HAADF images with corresponding magnifications B) 20 nm and C) 10 nm.

Alternatively, the procedure B was applied for preparation of Ag NPs. Et_3N was added drop-by-drop in both suspensions; the UV-vis spectra recorded from the samples after each addition of Et_3N are shown in SI-Figure 4. During the drop-by-drop reduction process, the plasmon band for sample Ag-BEA-2 broaden significantly. The maximum of the plasmon band is shifting to the red in the course of the reduction while its red-tail shows a continuous shift upwards. This spectral shape and evolution of the plasmon band indicate the formation of large Ag NPs (> 20 nm); the red-component is a contribution of the higher multipoles in the Mie scattering formulation. The same spectral evolution for sample **Ag^+-BEA-1** was obtained applying the procedure B. The formation of silver nanoparticles with a

diameter of 30 nm aggregated at the surface of zeolite crystals is observed (SI-Figure 4). This last sample was further investigated by pump-probe spectroscopy and was named **Ag^0-BEA-1b.** The zeolite suspensions reduced by method B are stable for few days only.

Ultrafast electrons-phonons photodynamics in sample Ag^0-BEA-1

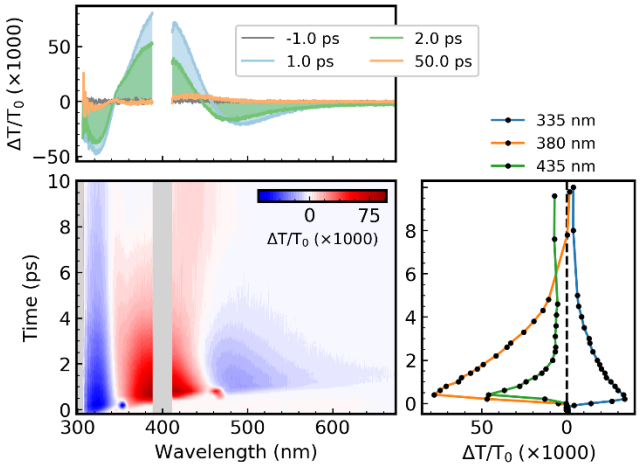

Figure 5. Transient absorption data recorded upon photo-excitation of sample Ag_0-BEA-1 at λ_{pump} =400 nm. 2D map of the transmission changes (bottom-left), transient spectra at representative pump-probe delays (top) and selected kinetics reconstructed from the transient spectra (bottom-right).

The femtosecond UV-vis transient absorption measurements on the three samples (**Ag^0-BEA-1, Ag^0-BEA-2 and Ag^0-BEA-1b)** were performed to characterize the hot-electrons photodynamic. The transient data recorded upon the photoexcitation of sample **Ag^0-BEA-1** are shown in **Figure 5** (λ_{pump}= 400 nm, I = 3 µJ (approximately 1.2 mJ/cm^2)). The optical response immediately after the absorption of the laser pump pulse (Δt ~ 200 fs) consists a strong positive transmission change in the spectral region of the plasmon resonance (400 nm); two weaker absorption contributions at 500 nm and 320 nm are observed. This transient signal is decaying within 5 ps without any significant evolution of its spectral profile. In the red-part of the plasmon band a rapid shift and narrowing of the absorption band is observed. While in the blue part below 400 nm, the absorption and the bleach contributions decay concomitantly with an isobestic point located at 340 nm. At longer pump-probe delays (**Figure 5**, Δt = 50 ps), the initial signal disappeared and replaced by a weak but clearly distinguishable absorption component bellow 340 nm, a bipolar-like signal with a negative lob at 370 nm and a positive one at 440 nm. This long-term transient absorption signal is slowly decaying within several hundreds of picoseconds (not shown). These two consecutive steps can be assigned as follow: the first short-lived contribution up to 5 ps agrees well with the transient spectra reported for photoexcited Ag NPs (see the review of Hartland[25] and references therein). The spectral components above 350 nm reflect the modification of the plasmon resonance resulting from formation of hot-electrons, while the component observed at higher energy (bellow 350 nm) is due to the perturbation of the inter-band optical transitions. The latest corresponds notably to the novel optical absorption resulting from the depletion of energy level below the Fermi energy (E_f). The lifetime of this signal (less than 5 ps) is characteristic with a decay governed by electron-phonon coupling following a photoexcitation under high-excitation regime[27,47]. The second long-term contribution (Δt = 50 ps and longer), features the blue shift of the plasmon band and a small depletion of the conduction band bellow E_f. Similar transient spectra have been assigned to the change of the dielectric constant induced by a local increase of the temperature around the nanoparticles[48]. In our experiments, the pump intensity was kept low enough to avoid any permanent change resulting from a strong heating of the Ag NPs or of its surrounding, as that was observed in photothermal or optical limitation[49] experiments. Based on the transient spectra, we verified that the photoexcitation of **Ag^0-BEA-1** induces the formation of hot electrons that dissipate their energy within a few picoseconds into the metal lattice that induces a limited transient perturbation of the surrounding media. Because this behavior is essentially similar to that observed for bare Ag NPs, we concluded that Ag NPs stabilized in the **Ag^0-BEA-1** sample are exhibiting essentially a metallic character.

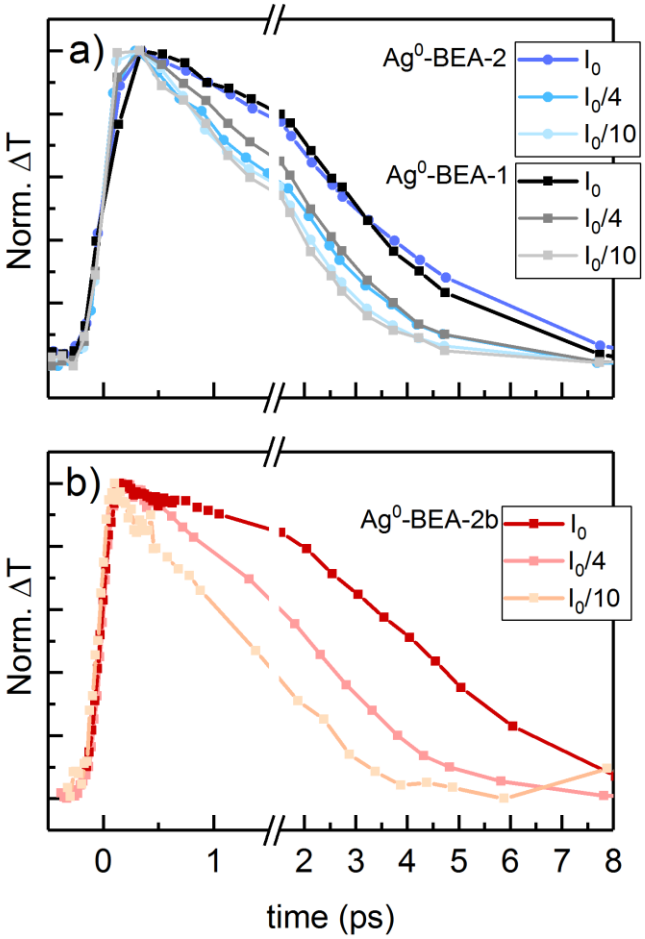

Figure 6. Kinetics of the transmission change probed at λ_{probe} = 380 nm, with different pump intensity (λ_{pump} = 400 nm), a) I_0 = 1.2 mJ/cm^2, Ag^0-BEA-1 and Ag^0-BEA-2, and b) I_0 = 1.2 mJ/cm^2, Ag^0-BEA-2b.

In order to go beyond the qualitative characterization of the process, we were interested in revealing the influence of the zeolite micro-environment on the electronic properties of the embedded Ag NPs. In particular, one point we wanted to address concerns the possible perturbation of the hot electron decay. Indeed, such a perturbation might be interpreted formally as a signature of the interaction of the hot-electrons with the electronic levels of the zeolite framework containing the organic template (TEA^+), Et_3N and water molecules. The transient spectra of **Ag^0-BEA-1** were measured following the method already applied for characterization of silver nanoparticle[24,26,47]. The samples were excited at 400 nm with different pump intensity varying from I_0 to I_0/20, with I_0 = 1.2 mJ/cm^2 (the intensity of the incident light on the sample). The electrons-phonons dynamics has been followed at the probe wavelength of 380 nm (3.25 eV). That probe energy lies well below the threshold of the inter-band transition of silver (322 nm, 3.85 eV) and it is in quasi-resonance with the plasmon. At this probe wavelength, for silver, the transmission changes are considered as being roughly proportional to the excess of internal energy of the gas of electrons.[47] The transmission changes recorded upon different laser intensities at λ_{probe}=380 nm are plotted in **Figure 6-a** and in **SI-Fig-7**. The amplitude of the transient signal and the hot electrons lifetime are decreasing when the intensity of the pump is reduced. This behavior is qualitatively in good agreement with a thermal exchange of energy between the excited hot electrons and the metal lattice. The data were fitted using a sum of exponential functions (See SI 2.2). All the decays are well reproduced by a major contribution (τ_1 ~ 1-3 ps) counting for more than 80 % of the signal and by a second minor component (τ_2 ~ 10 ps)**.** The use of two exponential decays in the fit function (see SI) reflects the dependency of the heat capacity of the electron with the temperature. From the fitted curves, we deduced the hot-electron apparent lifetime as the the time t(1/e) where the intensity of the transient signal has decreased by the factor 1/e. The value t(1/e) allows us to compare the kinetics between the different samples and excitation conditions. At the highest pump intensity, the Ag NPs with a size 1-2 nm can absorb several electron-volt per nanometer-cube, and consequently the electron temperature, Te, can reach thousands of Kelvin. This corresponds to a hot electron lifetime in the range 2-3 ps. At the lowest laser intensity (I_0 = 30 µJ/cm^2), Te is only a few hundreds of Kelvin and a decay time t(1/e) = 0.9 ps is measured that is close to the electrons-phonons coupling time-constant limit reported for silver nanoparticles (0.8-1.1 ps)[24,47,48].

Ultrafast electrons-phonons photodynamics in samples Ag^0-BEA-2 and Ag^0-BEA-2b

The same pump-probe measurements have been performed on samples **Ag^0-BEA-2** and **Ag^0-BEA-2b**. For sample **Ag^0-BEA-2**, the time-resolved spectra (SI, Figure 6) are qualitatively similar to the data reported for **Ag^0-BEA-1** (**Figure 5**), attesting for the formation and decay of hot-electrons in the metal nanoparticles. In **Figure 6-a,** the decays were recorded for pump-probe conditions (intensities and overlap) identical to that of sample **Ag^0-BEA-1** (**Figure 6-a**). At high intensity (I_0), we can notice that the decay is longer for the Ag^0-BEA-2 while at lower intensity, the difference between the two samples is less significative. However, for both samples, we are pointing out the fact that reducing the laser intensity from I_0/4 to I_0/10 has a relatively weak impact on the decay time. This effect is usually observed in case of coupling between the hot-electrons and its surrounding[29,50].

The transient spectra of sample **Ag^0-BEA-2b** are presented in SI-Figure-6. While a significant difference in the steady state absorption was found (**Figure 3** and SI-Figure 4) in comparison with the two other samples, the transient spectra are qualitatively similar to those obtained for **Ag^0-BEA-1** and **Ag^0-BEA-2**. We noticed however the absence of a residual contribution at long time-scale, which suggests that less perturbation of the surrounding of the nanoparticles occurs during the cooling process of the metal lattice. Regarding the photodynamic of sample **Ag^0-BEA-2b**,(Figure 6-b, SI-Figure 7 and 10), the hot-electrons lifetime measured under high excitation intensity (I_0 = 1 mJ/cm^2) is significantly longer than for the two other samples. In comparison with **Ag^0-BEA-1 and Ag^0-BEA-2**, we clearly observe the acceleration of the decay while the pump intensity is decreasing as expected for the silver nanoparticles with a size of 10-20 nm

Discussion

The results reported in the previous sections have allowed us to demonstrate: (1) the stabilization of Ag NPs in nanosized BEA zeolite matrix and (2) the metallic character of these Ag NPs evidenced by the formation of hot-electrons upon photo-excitation. In this section, we will discuss the effects of the preparation on the ultrafast optical and electronic response of the **Ag-BEA-1 and Ag-BEA-2** samples. As mentioned in the introduction, zeolites are materials of choice for the stabilization of metal clusters and metal nanoparticle due to the spatial constraints of their framework. In addition, the presence of organic templates, TEA^+ in the channels of BEA zeolite can also influence the growing process of silver nanoparticles in two ways. First, by controlling the initial distribution of Ag^+ introduced inside the zeolite, and second by hindering the diffusion of oligomers and nascent nanoparticles. The amount of silver cations introduced in both **Ag^+-BEA-1** and **Ag^+-BEA-2** samples by ion-exchange was relatively low (**Table 1)**, with an average ratio of 0.15-0.2 Ag^+/Al. So, only a small part of the charge compensating TEA^+ cations initially incorporated in the zeolite have been ion-exchanged with the silver whose final concentration in the zeolite is 1.2 Ag^+/u.c. and 0.6 Ag^+/u.c for samples **Ag^+-BEA-1** and **Ag^+-BEA-2,** respectively. After the reduction, the plasmon band at 410 nm for both samples was measured; the samples were stable for months (SI-Figure-4). We estimated the amount of reduced silver based on the optical density at the maximum of the plasmon band using the extinction coefficient of 9200 Lmol^{-1}cm^{-1} for silver atoms[46] and the concentration of Ag^+ in the samples determined by ICP. Within the accuracy of the extinction coefficient, which can vary with the size and shape of Ag NPs, we found that the percentage of reduced silver is in the range 90-95 %. It shows the high efficiency of our reduction procedure, and a relatively high accessibility of the Ag^+ cations. In our experiments, the formation of silver nanoparticles was taking place on the time scale of hours, however the reduction kinetics for the two samples was different. This can be explained with the different cation distribution, mobility or even chemical interactions for the two samples. The TG/DTG measurements (**Figure 2**) provide us the first evidence of different micro-environment. The TEA^+ and water content in samples **Ag^+-BEA-1** and **Ag^+-BEA-2** are 14.6 wt% / 1.0 wt% (TEA / water) and 17.3 wt% / 4.7wt%, respectively. Sample **Ag^+-BEA-1** is more hydrophobic, and contains less organic template and water in comparison to sample **Ag^+-BEA-2,** that can be explained with the different amounts of defects (surface and bulk) (**Figure 2**). For **Ag^+-BEA-2**, an increase of the total mass lost, mainly associated with a decrease of the water content, and an increase of the amine residues is observed. This corresponds probably to the incorporation of Et_3N, replacing partially or totally the water molecules. Interestingly, the presence of two new additional sharp peak at 220 and 226 °C was noticed (**Figure 2-d**) that we tentatively assigned to the Et_3N molecules in the vicinity of the Ag NPs.

Another important finding is to report the formation of Ag NPs in zeolite matrix with remarkable distinction in size using two reduction procedures (see procedures A and B). HRTEM images have revealed the formation of small Ag nanoparticles with a size typically 1-2 nm and dispersed homogeneously in the zeolite matrix using the procedure A. While the reduction of **Ag^+-BEA-1** and **Ag^+-BEA-2** under drop-wised addition of Et_3N (procedure B) favored the formation of unstable larger Ag NPs (20-30 nm). More than one hour was necessary to achieve the complete reduction of cationic Ag^+ into Ag NPs (**Figure 2**). By following the procedure A, reduction in excess of Et_3N, the concentration of reduced silver atom is kept at its maximum during the process so that the rapid formation of dispersed nucleation centers is favored. In opposite, following procedure B, the kinetics of formation of Ag NPs is comparable to the diffusion time, and the Ag NPs can escape and coalesce as extra-framework nanoparticles. This observation is in a good agreement with the mechanism of growth of colloidal metal nanoparticles for which the faster is the creation of nucleation centers, the smaller are the formed nanoparticles. [36,51,52] The growth of metal nanoparticles in zeolite follows the same principle and the final shape and size of the NPs is the results of the initial stabilization of the small oligomeric clusters[8,34,35] tailored by the channels and porous volume followed by a slow diffusion and structural rearrangement[35]. For Ag-BEA, it appears that the rapid formation of the initial nucleation centers is a determining step to keep the final size of the Ag-NPs in the 1-2 nm range.

In the last part of the discussion we will address the consequences of the different method of preparation employed in this work on the plasmonic response of Ag NPs in BEA zeolite. The steady state and time-dependent optical response of metal nanoparticles are governed by the collective properties of the electrons that depend directly on the density of electronics states (DOS) of the metal and its surrounding. The consequence is that the photodynamic of the electrons can reflect the electronic properties and interaction of the metal nanoparticles embedded in the zeolite. The measured hot electrons decays time t(1/e) versus the pump laser intensity for the three samples are depicted in **Figure 7**.

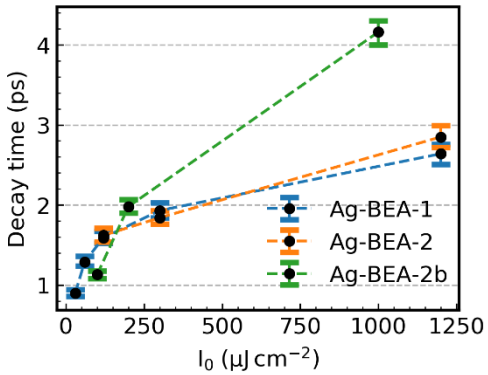

Figure 7. Electron-phonon decay time, t(1/e), deduced from the fit of the kinetic at λ_{probe}=380 nm for different laser intensity (λ_{pump} = 400 nm).

In metal nanoparticles, the energy absorbed by the electrons is transferred to the metal lattice by electron-phonon coupling. In this process, the hot electron lifetime increases with the amount of absorbed energy due to the temperature dependency of the electronic heat capacity. Our three samples qualitatively follow this trend, but we clearly observe distinct behaviors in both the profile of the curves and in the values of τ. First, the hot electron lifetimes recorded for the highest pump intensities (I > 250 μJ/cm^2) are significantly longer for **Ag^0-BEA-2b** (2-4 ps) than for **Ag^0-BEA-1** (1.6-2.85 ps) and **Ag^0-BEA-2** (1.6-2.64 ps). This observation must be associated with the fact that in **Ag^0-BEA-2b** the Ag NPs exhibit a larger size (>20 nm) in comparison with the two other samples for which the size is limited in the range 1-2 nm. The variation of the hot electron decay with the size of noble nanoparticles can be attributed to two main processes. The first explanation is based on the hypothesis of a higher thermal conductance, or vibrational coupling, at the interface of the metal which favor the transfer of energy from the metal lattice to its surrounding[24]. In this case, the observed lifetime would represent the time for the thermal transfer of energy from the hot electron to the surrounding of the metal. This hypothesis is supported by the transient spectra recorded after 10 ps for samples **Ag^0-BEA-1** and **Ag^0-BEA-2** shown in **Figure 5** and SI Figure 5. A long-living signal typical of the perturbation of the plasmon band induced by a local change of the temperature is expected[48]. The second possible explanation is based on the hypothesis of ultrafast interactions (< 100 fs) between the surface plasmon, by chemical interface damping, or between the highly excited electrons, by charge transfer, with the molecular species at the surface of the Ag NPs.[18,19,30] Both mechanisms result in the transfer of a part of the energy of the photon and in the subsequent reduction of the energy deposited in the hot electron. Consequently, the decay time is also reduced. Theoretical calculations[59] showed that the close proximity between the energy level of the Ag atoms and of the zeolite matrix support this scenario.
To further validate that the difference in the hot electron lifetime between samples **Ag^0-BEA-1** and **Ag^0-BEA-2**, and the sample **Ag^0-BEA-2b** is due to a size effect, we also performed a direct comparison with the plasmonic response of bare Ag NP (10 nm) stabilized in PVA/water solution. The hot electron dynamics was measured for this sample (Ag-PVA) and the **Ag^0-BEA-1** under rigorously equivalent laser intensity and pump-probe overlap. The results show clearly the acceleration of the decay in the **Ag^0-BEA-1** sample (**Figure 8**). This confirms that in **Ag^0-BEA-1** and **Ag^0-BEA-2** the hot electron dynamics is faster than in bulk silver nanoparticle. This suggests that the hot-electrons decays is not proceeding only by electron-phonon coupling but it is governed by the interaction at the interface of the metal.

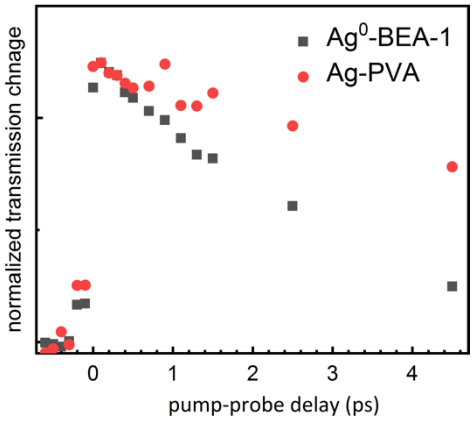

Figure 8. Comparison of the kinetic recorded with λ_{probe} = 380 nm for Ag^0-BEA-1 and Ag-PVA samples (normalized transient absorbance).

At the lowest excitation, we notice the reverse situation: the hot-electron lifetime is longer for the small Ag NPs (**Ag^0-BEA-1 , Ag^0-BEA-2**) than for the **Ag-BEA-2b**. Bauer and co-workers[29,30,50] reported that the gold nanoparticles in strong interactions (chemisorption) with sulfate molecules show hot electron decay time in weak perturbation regime equals to 1.7 ps independently of the pump intensity. The confinement of the molecules (water, Et_3N, TEA^+) in the BEA zeolite, or the zeolite framework itself, might favor the chemical

interface damping. The UV-vis spectra of **Ag^0-BEA-2**, exhibiting an absorption in the red wing of the plasmon band (**Figure 3**) support the existence of a charge transfer at the surface of the metal. The chemical interface damping has been recognized as an efficient mechanism to promote the photocatalytic activity of metal nanoparticles.
The influence of the chemical reduction route on the hot electron relaxation mechanism of Ag-BEA samples is represented schematically in **Figure 9**.
The nanosized Ag NPs stabilized by the BEA zeolite, due to their high surface-volume ratio are in a favorable situation for application in plasmonic chemistry. The results show that by controlling the size of Ag NPs using the confinement effect of zeolites can be of great interest for designing efficient photoactive materials.

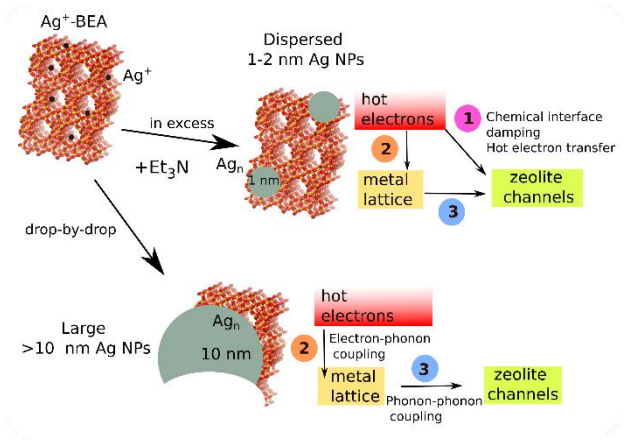

Figure 9. Influence of the chemical reduction route on the hot electron relaxation mechanism in Ag-BEA samples.

Conclusion

In this work, we present the preparation of silver nanoparticles in nanosized BEA type zeolite stabilized in colloidal suspensions. We demonstrated that after the introduction of silver cations (Ag^+) by ion exchange, nm-sized silver particle can be formed by instantaneous chemical reduction using an excess of trimethylamine. The photo-dynamics of the hot electrons in two BEA zeolite samples was characterized by femtosecond pump-probe transient absorption measurements in transmission, owing to the stability and transparency of the zeolite colloidal suspensions. The hot electron dynamics of Ag NPs embedded in the BEA zeolite matrix is strongly governed by the interactions at the surface of the metals. The capacity of the BEA zeolite to stabilize 1-2 nm-size Ag NPs is advantageous since the small sized Ag NPs increase the density of energy absorbed by the metals and it raises the surface interactions. However, the exact nature and mechanism of these chemical interface interactions is difficult to be predicted regarding the complexity of the zeolitite frameworks. More systematic time-resolved experiments in combination with advanced material characterizations will be beneficial to optimize these particular class of photoactive zeolites.

Experimental Section

Preparation of zeolite Beta colloidal suspensions

In this work two types of zeolite Beta samples, **BEA-1** and **BEA-2** of different Si/Al ratios have been investigated. Zeolite Beta nanocrystals were prepared under hydrothermal conditions from clear precursor suspensions with molar composition 9TEAOH: $0.5Al_2O_3$: $25SiO_2$: $295H_2O$ (**BEA-1**) and 9TEAOH: $0.25Al_2O_3$: $25SiO_2$: $295H_2O$ (**BEA-2**). Tetraethylammonium hydroxide (TEAOH) was used as an organic template for the preparation of BEA. Initially, the source of alumina (aluminium iso-butoxide, Al_2O_3) was dissolved in a solution containing TEAOH and distilled water, and then the silica source (colloidal silica 30 wt%) was added into the mixture under stirring. The precursor suspension was stirred for 60 minutes, and then subjected to hydrothermal treatment at 100 °C for 3 days. The obtained crystalline suspension was then purified by multistep high-speed centrifugation (20 000 rpm, 1 h) till a pH of the decanting solution of 9 was reached. The purified zeolite samples were redispersed in distilled water.

Preparation of Ag^+ containing zeolite Beta nanocrystals by ion-exchange process

The BEA zeolite colloidal suspensions were mixed with 0.5 $mol.l^{-1}$ $AgNO_3$ and continuously stirred for 3 hours at room temperature. The obtained suspensions were purified twice using high speed centrifugation (10 000 rpm, 60 mn) by adding water upon each centrifugation step to remove excess of free silver. The recovered nanocrystals were redispersed in water with a concentration of solid (zeolite) particles of 0.8 wt% and pH=7. The ion-exchanged samples are denoted as **Ag^+-BEA-1** and **Ag^+-BEA-2**.

Preparation of Ag NPs in colloidal zeolite BEA by chemical reduction method:

Wet chemical reduction procedure towards preparation of Ag NP in the zeolite suspension was applied. Triethylamine (denoted as Et_3N) was dissolved in ethanol (EtOH) and stirred for few minutes in order to ensure its complete dissolution. Two chemical reduction procedures were implemented: Method A: Fast one-step chemical reduction procedure, in which Ag^+-BEA-1,-2 (0.8wt%) samples were added directly to the Et_3N mixture (Et_3N : EtOH ratio 1 : 5) under continuous stirring at room temperature (Ag^+-BEA-1, -2 : Et_3N ratio 3.33 : 1). The suspensions were further stirred for one hour. The obtained samples will hereafter be denoted as **Ag^0-BEA-I** and **Ag^0-BEA-2**. Method B: Slow drop-by-drop chemical reduction procedure, in which Et_3N mixture (Et_3N : EtOH ratio 1:1) was added slowly to a diluted suspensions of ion-exchanged **Ag^+-BEA-1, -2** samples containing 0.032wt % of solid (zeolite) particles using micropipettes under vigorous stirring.

Preparation of pure Ag NP colloidal suspension stabilized by polyvinyl alcohol (PVA)

Ag-NPs were prepared according to the procedure described in ref [46]. The solutions were made using ultra-pure water from a Millipore system (18 MΩ cm) and reagent-grade chemicals without further purification: $AgClO_4$ and poly(vinyl alcohol) (PVA, 99% hydrolysed, MW=86000) from Aldrich, 2-propanol from Prolabo. The solutions were de-aerated by bubbling with nitrogen (N_2, Air Liquide) before irradiation. All the aqueous samples were kept at natural pH. The *γ*-irradiation source was a ^{60}Co *γ*-facility of 7000 Curies with a dose rate of 1.75 Gy s^{-1} (6300 Gy h^{-1}). The composition of the solution exposed to *γ*-rays was 2×10^{-3} M $AgClO_4$, 0.1 M PVA and 2 M 2-propanol. This procedure leaded to the formation of Ag-NPs with an average size of 20 nm characterized by a maximum of absorbance at 412 nm (ε_{412}=9200 dm^3 mol^{-1} cm^{-1}).

Characterization

Powder X-ray diffraction (XRD) patterns were recorded in Debye-Scherrer geometry using a Siemens D5005 or PANalytical X'Pert Pro diffractometer with Cu Kα radiation (λ=1.5418 Å). Prior XRD experiments, the zeolite colloidal suspensions were freeze-dried, and the powders obtained were homogenized and spread on silicon holders. The samples were scanned in 2θ range of 3-50° with a step of 0.028° and 2.5 minute/degree step time.

The morphological features of zeolite nanocrystals were visualized by scanning electron microscopy (SEM) recorded with TESCAN-MIRA field-emission scanning electron microscope operating at 30 kV. Before carrying out the measurements, samples in powder form were coated with a thin layer of conducting material (platinum or gold) to improve the electrical conductivity using CRESSINGTON sputter machine. Additionally, the morphology, crystallinity and size of both zeolite BEA nanocrystals and Ag NPs were characterized using High Resolution Transmission Electron Microscopy (TEM). TEM micrographs and HADDF measurements were performed using a 200 kV JEOL 2010 FEG STEM electron microscope equipped with EDAX Energy Dispersive Spectrometer (EDS). In order to lower beam damages on samples low dose conditions were used for the images recording.

The particles size distribution and the stability of zeolite colloidal suspensions (0.12 wt% of solid particles) were measured by Dynamic Light scattering (DLS). DLS curves were recorded by Malvern Zetasizer Nano Series DLS instrument. The chemical composition of the samples was determined by Inductively Coupled Plasma-Atomic Emission Spectrometry (ICP) using a Varian ICP-OES system. Thermogravimetric (TG/DTG) analyses were performed to determine the amount of organic template and water in the zeolite samples with and without silver. TG/DTA analyses were measured using a SETSYS evolution instrument (SETARAM). The measurements were carried out on ~10 mg of sample under air with a flow rate of 40 $ml.min^{-1}$. The nitrogen adsorption-desorption measurements were recorded on samples calcined under vacuum at 500 °C. N_2 sorption isotherms were measured using Micromeritics ASAP 2020 analyzer.

The UV-vis absorption spectra were recorded from the colloidal zeolite suspensions containing Ag NPs in quartz cuvettes of 1 cm path length using a Carry 4000 spectrometer working in transmission mode.

Femtosecond transient absorption measurements

UV-vis femtosecond transient absorption measurements were performed using the experimental set-up described in ref[54]. Briefly, the laser pump excitation (λ_{pump} = 400 nm) was generated by frequency doubling of the fundamental emission at 800 nm from the Ti:Sa amplifier (Libra Coherent) using a BBO crystal. A white light super continuum probe covering the 320-800 nm spectral range was generated by focusing a few µJ of the fundamental laser pulses at 800 nm into a moving CaF_2 plate. The transient spectra are recorded using a LN2-cooled CCD camera (Princeton Instrument).

The measurements were performed in quartz cuvettes with an optical path 1 cm or using a flow cell with an optical path of 1 mm. No photodegradation of the Ag-BEA suspensions during the experiments was observed; the measurements in the static cell were preferred as considered to be less invasive. The electron-phonon dynamics is determined by the initial quantity of light absorbed by the sample. Thus, special attention was paid to keep the pump-probe overlap conditions unchanged when comparing the photodynamic at different pump intensity or between different samples. At least two samples were measured per day for cross-referencing of the data.

Acknowledgements

Financial support from the Chevreul institutes (FR 2638), the Ministère de l'Enseignement Supérieur et de la Recherche, Région Nord – Pas de Calais and FEDER is acknowledged.

Keywords: pump-probe spectroscopy • plasmonic • zeolite • silver nanoparticle • hot electron

[1] S. Hashimoto, *J. Photochem. Photobio. C: Photochemistry Reviews* **2003**, *4*, 19–49.
[2] N. Alarcos, F. Sánchez, A. Douhal, *Microporous Mesoporous Mater.* **2017**, *248*, 54–61.
[3] S. Mintova, V. De Waele, M. Hölzl, U. Schmidhammer, B. Mihailova, E. Riedle, T. Bein, *J. Phys. Chem. A* **2004**, *108*, 10640–10648.
[4] M. R. di Nunzio, E. Caballero-Mancebo, C. Martín, B. Cohen, M. T. Navarro, A. Corma, A. Douhal, *Microporous Mesoporous Mater.* **2018**, *256*, 214–226.
[5] Y. Leydet, F. J. Romero-Salguero, C. Jiménez-Sanchidrián, D. M. Bassani, N. D. McClenaghan, *Inorg. Chim. Acta* **2007**, *360*, 987–994.
[6] A. Corma, V. Fornés, M. Galletero, H. García, J. C. Scaiano, *ChemComm* **2002**, *2*, 334–335.

[7] W. Baekelant, S. Aghakhani, E. Coutino-Gonzalez, K. Kennes, F. D'Acapito, D. Grandjean, M. Van Der Auweraer, P. Lievens, M. B. J. Roeffaers, J. Hofkens, J. A. Steele, *J. Phys. Chem. Lett.* **2018**, *9*, 5344–5350.
[8] O. Fenwick, E. Coutiño-Gonzalez, D. Grandjean, W. Baekelant, F. Richard, S. Bonacchi, D. De Vos, P. Lievens, M. Roeffaers, J. Hofkens, P. Samorì, *Nat. Mater.* **2016**, *15*, 1017–1022.
[9] D. Brühwiler, G. Calzaferri, *Microporous Mesoporous Mater.* **2004**, *72*, 1–23.
[10] G. Calzaferri, K. Lutkouskaya, *Photochem. Photobiol. Sci.* **2008**, *7*, 879–910.
[11] A. Corma, H. Garcia, *ChemCom* **2004**, *4*, 1443–1459.
[12] M. Matsuoka, M. Anpo, *J. Photochem Photobio. C: Photochemistry Reviews* **2003**, *3*, 225–252.
[13] H. H. Patterson, R. S. Gomez, H. Lu, R. L. Yson, *Catal. Today* **2007**, *120*, 168–173.
[14] P. Zhang, T. Wang Dr., J. Gong, *Adv. Mat.* **2015**, *27*, 5328–5342.
[15] X. Zhang, X. Ke, A. Du, H. Zhu, *Sci. Rep.* **2014**, *4*.
[16] S. Sohrabnezhad, A. Rezaei, *Superlattices Microstruct.* **2013**, *55*, 168–179.
[17] P. Christopher, H. Xin, S. Linic, *Nat. Chem.* **2011**, *3*, 467–472.
[18] P. Christopher, H. Xin, A. Marimuthu, S. Linic, *Nat. Mat.* **2012**, *11*, 1044–1050.
[19] C. Frischorn, M. Wolf, *Chem. Rev.* **2006**, *106*, 4207–4233.
[20] J. Y. Park, S. M. Kim, H. Lee, I. I. Nedrygailov, *Acc. Chem. Res.* **2015**, *48*, 2475–2483.
[21] C. Voisin, D. Christofilos, P. A. Loukakos, N. Del Fatti, F. Vallée, J. Lermé, M. Gaudry, E. Cottancin, M. Pellarin, M. Broyer, *Phys. Rev. B* **2004**, *69*, 195416-1-195416–13.
[22] N. Del Fatti, C. Voisin, M. Achermann, S. Tzortzakis, D. Christofilos, F. Vallée, *Phys. Rev. B* **2000**, *61*, 16956–16966.
[23] J.-Y. Bigot, V. Halté, J.-C. Merle, A. Daunois, *Chem. Phys.* **2000**, *251*, 181–203.
[24] V. Halté, J.-Y. Bigot, B. Palpant, M. Broyer, B. Prével, A. Pérez, *Appl. Phys. Lett.* **1999**, *75*, 3799–3801.
[25] G. V. Hartland, *Chem. Rev.* **2011**, *111*, 3858–3887.
[26] J. H. Hodak, A. Henglein, G. V. Hartland, *J. Phys. Chem. B* **2000**, *104*, 9954–9965.
[27] J. H. Hodak, A. Henglein, G. V. Hartland, *J. Chem. Phys.* **2000**, *112*, 5942–5947.
[28] M. B. Mohamed, T. S. Ahmadi, S. Link, M. Braun, M. A. El-Sayed, *Chem. Phys. Lett.* **2001**, *343*, 55–63.
[29] C. Bauer, J.-P. Abid, H. H. Girault, *Chem. Phys.* **2005**, *319*, 409–421.
[30] C. Bauer, H. H. Girault, EQEC '05. European Quantum Electronics Conference, **2005**., Munich, p. 162-, doi: 10.1109/EQEC.2005.1567333
[31] H. Awala, J.-P. Gilson, R. Retoux, P. Boullay, J.-M. Goupil, V. Valtchev, S. Mintova, *Nat. Mater.* **2015**, *14*, 447–451.
[32] S. Mintova, M. Jaber, V. Valtchev, *Chem. Soc. Reviews* **2015**, *44*, 7207–7233.
[33] J. Kecht, Z. Tahri, V. De Waele, M. Mostafavi, S. Mintova, T. Bein, *Chem. Mater.* **2006**, *18*, 3373–3380.
[34] B. Dong, R. Retoux, V. de Waele, S. G. Chiodo, T. Mineva, J. Cardin, S. Mintova, *Microporous Mesoporous Mater* **2017**, *244*, 74–82.
[35] A. Souici, K.-L. Wong, V. De Waele, J. L. Marignier, T. H. Metzger, N. Keghouche, S. Mintova, M. Mostafavi, *J. Phys. Chem. C* **2014**, *118*, 6324–6334.
[36] J. Grand, S. R. Ferreira, V. De Waele, S. Mintova, T. M. Nenoff, *J. Phys. Chem. C* **2018**, *122*, 12573–12588.
[37] Z. Tahri, F. Luchez, I. Yordanov, O. Poizat, A. Moissette, V. Valtchev, S. Mintova, M. Mostafavi, V. De Waele, *Res. Chem. Intermed.* **2009**, *35*, 379–388.
[38] A. Kharchenko, O. I. Lebedev, V. Zholobenko, V. De Waele, S. Mintova, *J. Phys. Chem. C* **2016**, *120*, 26300–26308.
[39] F. Luchez, Z. Tahri, V. De Waele, I. Yordanov, S. Mintova, A. Moissette, M. Mostafavi, O. Poizat, *Microporous Mesoporous Mater.* **2014**, *194*, 183–189.
[40] M. Bryckaert, A. Kharchenko, O. Lebedev, B. Dong, I. De Waele, G. Buntinx, O. Poizat, S. Mintova, V. De Waele, *J. Phys. Chem. C* **2017**, *121*, 26958–26966.
[41] M. M. J. Treacy, J. B. Higgins, *Collection of Simulated XRD Powder Patterns for Zeolites Fifth (5th) Revised Edition*, **2007**.
[42] M. D. Kadgaonkar, M. W. Kasture, D. S. Bhange, P. N. Joshi, V. Ramaswamy, R. Kumar, *Microporous Mesoporous Mater.* **2007**, *101*, 108–114.
[43] F. Vaudry, F. D. Renzo, F. Fajula, P. Schulz, *Stud. Surf. Sci. Catal.* **1994**, *84*, 163–170.
[44] F. Vaudry, F. Di Renzo, P. Espiau, F. Fajula, Ph. Schulz, *Zeolites* **1997**, *19*, 253–258.
[45] E. Bourgeat-Lami, F. Di Renzo, F. Fajula, P. H. Mutin, T. Des Courieres, *J. Phys. Chem.* **1992**, *96*, 3807–3811.
[46] H. Remita, I. Lampre, M. Mostafavi, E. Balanzat, S. Bouffard, *Radiat. Phys. Chem.* **2005**, *72*, 575–586.
[47] C. Voisin, N. D. Fatti, D. Christofilos, F. Vallee, *J. Phys. Chem. B* **2001**, *105*, 2264–2280.
[48] J. H. Hodak, I. Martini, G. V. Hartland, *J. Phys. Chem. B* **1998**, *102*, 6958–6967.
[49] L. François, M. Mostafavi, J. Belloni, J. A. Delaire, *Phys. Chem. Chem. Phys.* **2001**, *3*, 4965–4971.
[50] C. Bauer, J. P. Abid, H. H. Girault, *Comptes Rendus Chimie* **2006**, *9*, 261–267.
[51] M. Mostafavi, J. L. Marignier, J. Amblard, J. Belloni, *Radiat. Phys. Chem.* **1989**, *34*, 605–617.
[52] J. Belloni, J.-L. Marignier, M. Mostafavi, *Radiat. Phys. Chem.* **2020**, *169*
[53] S. G. Chiodo, T. Mineva, *J. Phys. Chem. C* **2016**, *120*, 4471–4480.
[54] G. Buntinx, R. Naskrecki, O. Poizat, *J. Phys. Chem.* **1996**, *100*, 19380–19388.

Entry for the Table of Contents

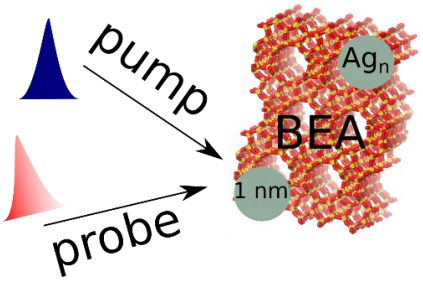

Silver nanoparticles with a size 1-2 nm have been prepared in colloidal zeolites. The plasmonic response was characterized by UV-vis femtosecond absorption spectroscopy and it has revealed that the hot electron lifetime is governed by interactions and couplings at the interface of the silver nanoparticle. Thus, the as-prepared samples are promising in the perspective of plasmonic chemistry applications.

Institute and/or researcher Twitter usernames: @CNRS @LasireTeamPCS @LCPlab @labo_LCS @univ_lille